Experimental characterization of a 400 Gbit/s orbital angular momentum multiplexed free-space optical link over 120-meters

YONGXIONG REN,[1,*] ZHE WANG,[1] PEICHENG LIAO,[1] LONG LI,[1] GUODONG XIE,[1] HAO HUANG,[1] ZHE ZHAO,[1] YAN YAN,[1] NISAR AHMED,[1] ASHER WILLNER,[1] MARTIN P. J. LAVERY,[2] NIMA ASHRAFI,[3] SOLYMAN ASHRAFI,[3] ROBERT BOCK,[4] MOSHE TUR,[5] IVAN B. DJORDJEVIC,[6] MARK A. NEIFELD,[6] AND ALAN E. WILLNER[1]

[1]*Department of Electrical Engineering, University of Southern California, Los Angeles, California 90089, USA*
[2]*School of Physics and Astronomy, University of Glasgow, Glasgow, G12 8QQ, UK*
[3]*NxGen Partners, Dallas, Texas 75219, USA*
[4]*R-DEX Systems, Marietta, GA 30068, USA*
[5]*School of Electrical Engineering, Tel Aviv University, Ramat Aviv 69978, Israel*
[6]*Department of Electrical and Computer Engineering, University of Arizona, Tucson, Arizona 85721, USA*
**Corresponding author: yongxior@usc.edu*

Received XX Month XXXX; revised XX Month, XXXX; accepted XX Month XXXX; posted XX Month XXXX (Doc. ID XXXXX); published XX Month XXXX

We experimentally demonstrate and characterize the performance of a 400-Gbit/s orbital angular momentum (OAM) multiplexed free-space optical link over 120-meters on the roof of a building. Four OAM beams, each carrying a 100-Gbit/s QPSK channel are multiplexed and transmitted. We investigate the influence of channel impairments on the received power, inter-modal crosstalk among channels, and system power penalties. Without laser tracking and compensation systems, the measured received power and crosstalk among OAM channels fluctuate by 4.5 dB and 5 dB, respectively, over 180 seconds. For a beam displacement of 2 mm that corresponds to a pointing error less than 16.7 μrad, the link bit-error-rates are below the forward error correction threshold of 3.8×10^{-3} for all channels. Both experimental and simulation results show that power penalties increase rapidly when the displacement increases. © 2015 Optical Society of America

OCIS codes: *060.2605 (Free-space optical communication); 060.4230 (Multiplexing); 999.9999 (Orbital angular momentum).*

http://dx.doi.org/10.1364/OL.99.099999

Free-space optical (FSO) communications has attracted much attention for a variety of applications, such as back-haul and data centers [1, 2]. Given the rapid growth of bandwidth demand for these applications, there is increased interest in utilizing advanced multiplexing of multiple data streams to increase the data capacity and spectral efficiency of an FSO system [3]. Multiplexing in wavelength and polarization, known as wavelength division multiplexing (WDM) and polarization division multiplexing (PDM) respectively, have previously been used for FSO transmission [3, 4].

Another potential approach is to use space division multiplexing (SDM), for which multiple beams each carrying an independent data stream are transmitted through a common medium [5, 6]. Provided these spatially-overlapping beams can be properly demultiplexed with tolerable crosstalk, the total capacity and spectral efficiency of the communication system is increased by a factor equal to the number of transmitted orthogonal modes. An orthogonal spatial modal basis set for SDM that has gained interest is orbital angular momentum (OAM) [5-8]. OAM beams with different ℓ values (ℓ is an unbounded integer) are mutually orthogonal [8, 9], so that beams carrying different OAM can act as independent data channels for efficiently multiplexing multiple information-bearing signals in an SDM-based communication system [5]. Moreover, similar to any SDM approach, OAM multiplexing is in principle compatible with existing WDM and PDM techniques [6]. We note that compared to other modal sets, such as Hermite-Gaussian (HG) modes that could also be used for SDM, OAM modes might offer the potential advantage of being conveniently matched to many optical subsystems due to their circular symmetry.

It is known that the amount of phase change per unit area for an OAM beam is greatest in the beam center, and that collecting sufficient phase changes is critical for ensuring orthogonality among OAM beams [9]. As a result, OAM multiplexing might be more sensitive to system alignment as it relies more critically on a common optical axis to achieve low inter-modal crosstalk [10]. OAM multiplexing has been employed to demonstrate high-capacity FSO transmission links in laboratory settings [6, 7]. These experiments were generally

conducted over short distances of ~1 meter, without taking into account system misalignment and other potential channel effects. Recent reports have shown the transmission of a single low-data rate OAM channel with no multiplexing over practical distances [11-14], including a 3-km link by encoding information in the intensity pattern of OAM superpositions [12]. However, the experimental study of the issues related to multiplexing and transmitting multiple OAM beams for high-speed FSO systems has not been reported so far.

In this paper, we explore the potential of using OAM multiplexing to achieve high-capacity data transmission beyond lab-scale distances. We experimentally demonstrate and investigate the performance of an FSO link employing OAM multiplexing that is performed over 120-meter on the roof of a building. Four OAM modes with ℓ = ±1, ±3, each carrying a 100-Gbit/s quadrature-phase-shift-keyed (QPSK) data channel are transmitted, thus allowing for a total capacity of 400-Gbit/s [15]. We measure the beam jitter (tip/tilt aberrations) of the link and characterize its effects on system performance. Without laser tracking and compensation system used at the receiver, the received signal power and crosstalk among the OAM channels fluctuate by 4.5 dB and 5 dB, respectively, over 180 seconds. For a beam displacement of 2 mm that corresponds to a pointing error less than 16.7 μrad, the bit-error-rates (BERs) of the link can achieve below the forward error correction (FEC) threshold of 3.8×10^{-3} for all channels. We vary the displacement of the received beams and we find that power penalties increase rapidly when displacement is increased, which is in agreement with our simulation results.

The experimental setup is presented in Fig. 1. The optical setup containing the transmitter and the receiver is placed on the roof of a building (shown in Fig. 1(a)), which is about 20-meter above the ground. The transmitter and the receiver are located on the same optical bench at Site #1. Two flat mirrors placed 30 meters away at Site #2 and a flat mirror on the optical bench at Site #1 are used to reflect the OAM beams twice, achieving a 120-meter propagation path, as shown in Fig. 1(b1). The transmitting and receiving apertures are around 40 cm apart from each other, so that the return paths do not coincide with the forward paths.

The OAM transmitter optics is shown in Fig. 1(b2). A 100-Gbit/s QPSK signal at 1550 nm is produced, amplified and split into two copies, one of which is delayed using a 10-meter length of single-mode fiber (SMF) to decorrelate the data sequence. These two polarized signal copies are sent to two collimators, each converting the SMF output to a collimated free-space Gaussian beam with a diameter of 3 mm. The two beams are launched onto two reflective spatial light modulators (SLMs 1 and 2 respectively), to create two different OAM beams with either ℓ = +1 or +3. These two OAM beams are spatially combined using a beam splitter (BS-1). The multiplexed OAM beams are then split into two identical copies by BS-2, one of which is reflected 3 times using mirrors arranged to introduce a ~300 ps delay between the two copies. Due to the "mirror" image relationship of reflection, the state number of an OAM beam changes its sign after an odd number of reflections [9]. As a result, another two OAM beams with opposite ℓ values (ℓ = -1 and -3) are obtained, which are then combined with the original OAM beams ℓ = +1 and +3 using BS-3. Next, the resulting four multiplexed OAM beams (ℓ = ±1 and ±3) are sent through a 1: 4 beam expander to enlarge their transmitted beam sizes. Specifically, the beam sizes become ~1.32 cm for OAM beams ℓ = ±1 and ~1.76 cm for ℓ = ±3. The expansion of transmitted beams is performed to ensure that most of the received OAM beams can be captured by the receiver aperture. Subsequently, the expanded OAM beams are combined with a red Gaussian beam at 635 nm, which serves as a beacon for the convenience of system alignment. This 635 nm beam has a 0.7 mm beam size and a ~25 mrad divergence angle.

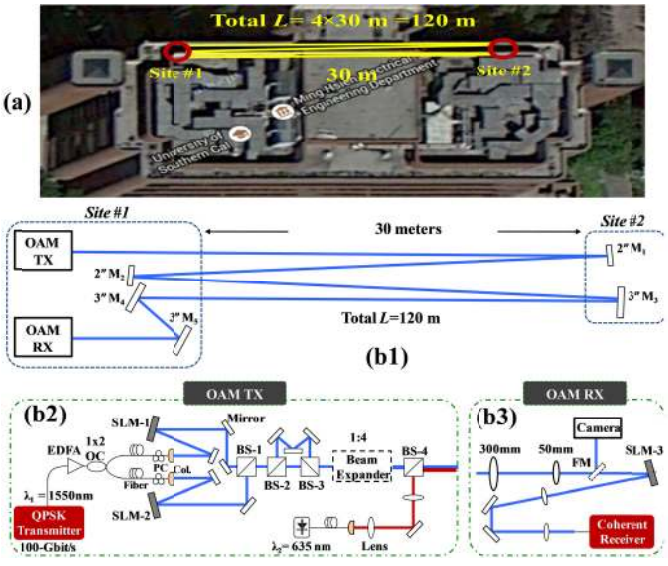

Fig. 1. Experimental setup of a 120-meter OAM-multiplexed link on a building roof. (a) Link layout on the building roof. (b1) Transmitter and receiver geometry, (b2) transmitter optics and (b3) receiver optics. BS: beam splitter, Col.: collimator, FM: flip mirror, M.: mirror, OC: optical coupler, PC: polarization controller. RX: receiver, TX: transmitter.

The OAM beams at 1550 nm and the Gaussian beam at 635 nm pass through a 2-inch transmitter aperture and then propagate for 30-meter in free-space. Two flat mirrors, with a diameter of 2-inch and 3-inch respectively, are mounted on an optical table at Site #2 to reflect the incoming beams twice towards the transmitter's direction. After three reflections and 120-meter propagation, the OAM beams ℓ = ±1 and ℓ = ±3 at the receiver have beam sizes of ~4.6 cm, and ~6.0 cm, respectively. In the receiver optics shown in Fig. 1(b3), the OAM beams are then collected by a beam reduction system, which has a 3-inch entrance aperture and consists of two lenses with focal lengths of 300 mm and 50 mm. The sizes of the OAM beams are reduced 6-fold to match the dimensions of SLM-based OAM detection module that followed. SLM-3 is loaded with the inverse spiral phase hologram that converts the OAM beam of a particular channel chosen for detection back into a flat-phase beam. After SLM-3, the other beams still maintain their ring-shaped profiles and helical phases. The flat-phase beam has a bright high-intensity at the beam center and is thus separable from the other beams through spatial filtering. This beam is then coupled into an SMF sent for coherent detection and off-line digital signal processing. Fiber coupling losses are ~6 dB for OAM ℓ = ±1 and ~8 dB for OAM ℓ = ±3, which can be potentially reduced by further optimization of the coupling optics. On the way from the beam reduction system to SLM-3, an infrared camera fed by a flip mirror is used to capture the intensity profiles of the received beams.

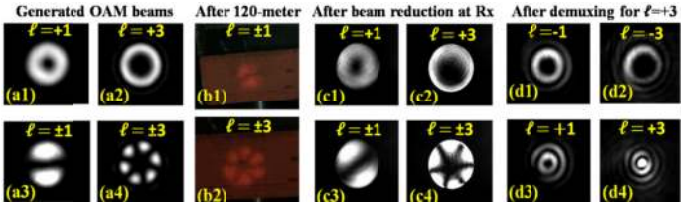

Fig. 2. Measured intensity profiles and superpositions of the OAM beams. Intensity profiles of (a) generated OAM beams (ℓ = +1, ℓ = +3, superpositions of ℓ = ±1, and ℓ = ±3) at transmitter, (b) received OAM superpositions of ℓ = ±1, and ℓ = ±3 after 120-meters, (c) OAM beams (ℓ = +1, ℓ = +3, and superpositions) after beam reduction at receiver, and (d) demultiplexed beams when SLM-3 is loaded with inverse spiral phases of either ℓ = -1, +1, -3 and +3 when only OAM channel ℓ=+3 is transmitted.

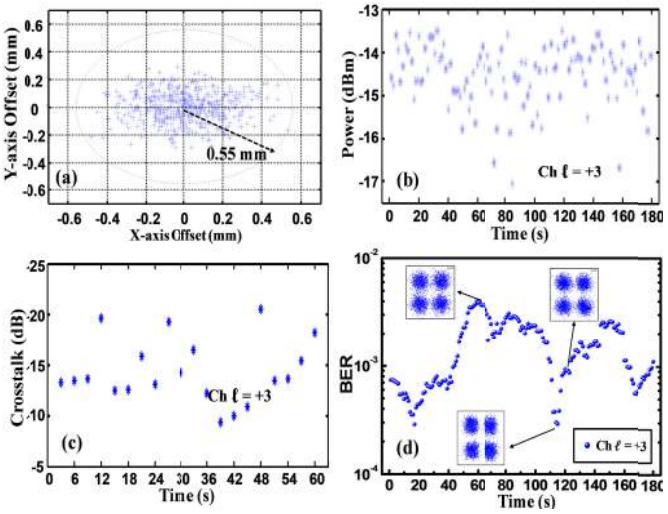

Fig. 3. Beam jitter and its effects on the received signal power, inter-channel crosstalk and instantaneous BER performance of OAM channel ℓ= +3. (a) Statistics of beam displacement at the CCD plane after 6-fold beam reduction with respect to the propagation axis due to platform vibration; the maximal displacement of the received beams is estimated to be ~3.3 mm. (b) The received signal power and (c) crosstalk from other channels for OAM channel ℓ = +3. (d) Instantaneous BERs of channel ℓ = +3 over 180 seconds at a fixed OSNR of 21 dB.

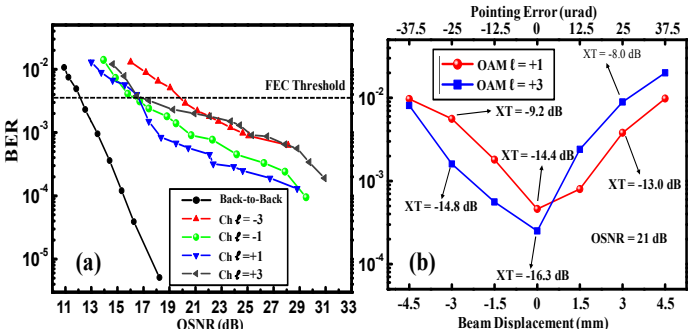

Fig. 4. (a) Measured BERs for all four OAM channels as a function of OSNR. (b) Measured BERs and crosstalk for OAM channels ℓ = +1 and ℓ = +3 as a function of beam displacement. XT: crosstalk.

The experimental measurements are performed under clear weather conditions at night. We expect that daylight would not significantly affect the system if the experiment is carried out during the daytime since daylight that resides in visible wavelength range can be filtered out by wavelength filters. Figure 2(a1-a4) shows captured intensity profiles of the generated OAM beams and their superpositions at the transmitter. After propagation over 120-meters, the sizes of the OAM beams ℓ = ±1 and ℓ = ±3 at the receiver are much larger than the effective area of the CCD camera. Therefore, we use a near-infrared detector card and a regular camera to capture their intensity profiles as shown in Fig. 2(b1-b2). The intensity profiles of the OAM beams and their superpositions after beam reduction are shown in Fig. 2(c1-c4). As the OAM beams ℓ = ±3 are of a similar size to the effective aperture of the receiver, an aperture diffraction effect caused by truncation is observed in Fig. 2(c2) and (c4). Figure 2(d1-d4) depicts the intensity profiles of demultiplexed beams when only the OAM channel ℓ= +3 is transmitted. We see that the received beam is converted into a flat-phase beam with a high-intensity at the beam center (Gaussian-like beam) only when an inverse spiral phase of ℓ = +3 is loaded onto SLM-3 for demultiplexing. It appears that the received beams do not suffer from atmospheric turbulence-induced distortions [16-19]. However, during the measurements we notice dynamic wandering of the beams at the receiver. This might result from the wind effects and time-dependent platform variations [20-22].

Due to beam jitter, the received power and crosstalk for each channel fluctuate [21, 22]. To quantify the beam jitter, we measure the statistics of beam displacement d with respect to the propagation axis after beam reduction, as depicted in Fig. 3(a). This is obtained by calculating the centroids of 1000 CCD image sequences (captured before SLM-3) of OAM beam ℓ= +3 over 180 seconds. It is observed that the maximum displacement at CCD plane is around 0.55 mm. Considering 6-fold beam reduction, the maximum beam displacement at the receiver is then estimated to be 3.3 mm, which corresponds to an angular pointing error of 27.5 μrad. The pointing error corresponding to displacement d, can be calculated by d/L with L =120 m being the link distance. The fluctuations of received signal and crosstalk from other channels into OAM channel ℓ = +3 are presented in Fig. 3(b-c). The crosstalk is calculated by measuring the received power values when only OAM channel ℓ = +3 is turned off and when only OAM channel ℓ = +3 is turned on. These two sequential measurements are performed every second and are repeated 60 times. The durations for power and crosstalk measurements are 180 and 60 seconds, respectively. We see that the signal power and crosstalk of channel ℓ = +3 vary by up to 3.8 dB and 10.2 dB respectively during this period. To illustrate the effects of beam jitter on system performance, Fig. 3(d) presents the instantaneous BERs of channel ℓ = +3 in 180 seconds at a fixed optical signal-to-noise ratio (OSNR) of ~21 dB. The recovered QPSK constellations of OAM channel ℓ = +3 under three different conditions are also shown in the inset. We see that the instantaneous BERs fluctuate temporally and link outage occurs (BERs larger than FEC threshold of 3.8×10^{-3}) under large jitter conditions. We emphasize that no laser tracking system is used in the experiment. Using such a system to stabilize the received beams would reduce the fluctuations and average values of channel crosstalk and system BERs.

Table 1. The power transfer over 5 minutes for each OAM channel.

Average Power	RX ℓ = -1	RX ℓ = +1	RX ℓ = -3	RX ℓ = +3
TX ℓ = -1	-8.5	-29.0	-26.3	-34.1
TX ℓ = +1	-27.5	-9.0	-27.5	-28.4
TX ℓ = -3	-22.5	-32.5	-11.3	-45.8
TX ℓ = +3	-34.5	-24.5	-43.2	-11

We then characterize the power leakage and crosstalk between all four OAM channels. The power leakage is measured in the following way: We first turn on OAM channel ℓ=+1 while all the other channels (OAM ℓ=-1 and ℓ = ±3) are off. Then we record the received power values when demultiplexing different OAM channels (the pattern loaded on SLM-3 is switched between inverse spiral phase holograms of ℓ = ±1 and ℓ = ±3). These measurements are then performed for all the other transmitted OAM channels, resulting in a full 4×4 power transfer matrix. The above measurements are repeated over 5-minute and an average power transfer matrix between the four channels, as shown in Table. 1, can be obtained by averaging all the 4×4 matrices measured during this period. The average crosstalk of a specific channel over this 5-minute period can be calculated from the average 4×4 power transfer matrix by adding the received power from all other channels divided by the received power of this channel.

Next, we turn on all four OAM channels and the measured BER curves are shown in Fig. 4(a). Each BER point is averaged over a 60 seconds period. Because of inter-channel crosstalk, the BERs for all four channel exhibit slight error-floor phenomenon. We see that the power penalties at the FEC threshold for all four channels ℓ = -3, -1, +1,

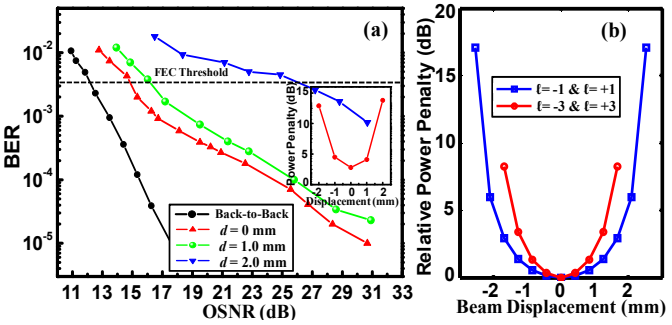

Fig. 5. BER and system power penalty under various beam displacements. (a) Measured BERs for OAM ℓ = +3 channel as a function of OSNR under various beam displacements; (b) Simulated power penalty for OAM channels ℓ = -3, -1, +1 and +3 under different beam displacements; this is calculated by using the simulation model established in [10].

and ℓ = +3, compared to the back-to-back case (bypassing the link setup) are 7.7 dB, 4.3 dB, 4.4 dB, and 4.6 dB, respectively. To investigate the maximal beam jitter that the system allows, we intentionally adjust the displacement of the received beams with respect to the receiver axis. In this case, the total misalignment is a combination of this static displacement and the random time-varying jitter. It is expected that this misalignment would cause power coupling among neighboring channels, resulting in inter-channel crosstalk. The measured BERs and crosstalk values for OAM channels ℓ = +1 and +3 at an SNR of 21 dB as a function of various lateral displacement are depicted in Fig. 4(b). It is found that a maximum beam displacement of ~2 mm (16.7 μrad pointing error) can be tolerated to achieve BERs below 3.8×10^{-3}.

Figure 5(a) shows the measured BERs (averaged over 60 second) for OAM channel ℓ = +3 under d = 0 mm, 1. 0 mm and 2.0 mm. We see that the BER performance degrades more rapidly when d is larger than 1.0 mm, which is also corroborated by the power penalty of OAM channel ℓ = +3 (at the FEC threshold) as shown in Fig. 5(a) inset. It is clear that the power penalty is larger than 10 dB at d = 2.0 mm. We also observe that power penalties increase rapidly when d is larger than 1.0 mm. In general, a pointing error of the order of μrad could be reduced to nrad level using a commercially available laser tracking system [10, 22, 23], which would improve system performance.

Figure 5(b) shows the simulated relative power penalty (compared to the case when there is no displacement) for all OAM channels as a function of lateral displacement when multiplexed OAM channels ℓ = ±1 and ℓ = ±3 are transmitted over 120-meters. This is obtained by applying the simulation model established in Ref. [10] with the link parameters of the experiment. We see that the simulation and experimental results share a similar trend, and power penalty increases dramatically as lateral displacement exceeds a certain value.

Our experiment was performed on a building roof under clear weather conditions and the effects of atmospheric turbulence seems to be weak according to our measured intensity profiles. The main channel impairment, namely beam jitter would be more severe over a longer distance or if the transmitter and receiver are placed on different buildings [20, 21]. Meanwhile, the increased turbulence effects in a longer link would introduce additional beam jitter (i..e, beam wandering). The beam jitter caused by the two factors, each with a temporal bandwidth of ~0.1-1 kHz [16] could be corrected with commercially available pointing and tracking control technology [23].

We believe that our experiment could be potentially scaled to a larger number of OAM channels over a km-long distance through careful system design [10]. In general, the number of accommodated OAM beams is limited by various factors, including aperture sizes and channel condition. Given a fixed transmitter and receiver aperture size, a larger OAM ℓ value results in a larger beam size at the receiver such that the recovered power decreases. In addition, atmospheric turbulence may present a critical issue for long-distance scenarios or under bad weather conditions [1, 16]. Turbulence-induced high-order aberrations cause degradation of the mode purity for each OAM beam, leading to changes in the received power of each OAM channel and inter-channel crosstalk behaviors [17-19]. This might severely limit the number of OAM beams that can be used for transmission. In this case, turbulence mitigation approaches might be required [24].

Funding. NxGen Partners; the Air Force Office of Scientific Research.

Acknowledgment. We thank Dr. Michael Kendra for fruitful discussions.

References

1. V.W.S. Chan, IEEE J. lightw. Tech. **24**, 4750-4762 (2006).
2. I. B. Djordjevic and M. Arabaci, Opt. Express **18**, 24722-24728 (2010).
3. E. Ciaramella, Y. Arimoto, G. Contestabile, M. Presi, A. D'Errico, V. Guarino, and M. Matsumoto, IEEE Photon. Technol. Lett. **21**, 1121-1123 (2009).
4. A. Turpin, Y. Loiko, T. K. Kalkandjiev, and J. Mompart, Opt. Lett. **37**, 4197-4199 (2012).
5. G. Gibson, J. Courtial, M. Padgett, M. Vasnetsov, V. Pas'ko, S. Barnett, and S. Franke-Arnold, Opt. Express **12**, 5448-5456 (2004).
6. J. Wang, J.-Y. Yang, I. M. Fazal, N. Ahmed, Y. Yan, H. Huang, Y. Ren, Y. Yue, S. Dolinar, M. Tur, and A. E. Willner, Nature Photonics **6**, 488-496 (2012).
7. T. Su, R. P. Scott, S. S. Djordjevic, N. K. Fontaine, D. J. Geisler, X. Cai, and S. J. B. Yoo, Opt. Express **20**, 9396-9402 (2012).
8. L. Allen, M. W. Beijersbergen, R. J. C. Spreeuw, and J. P. Woerdman, Phys. Rev. A **45**, 8185-8190 (1992).
9. A. Yao and M. J. Padgett, Adv. Opt. Photon. **3**, 161-204 (2011).
10. G. Xie, L. Li, Y. Ren, H. Huang, Y. Yan, N. Ahmed, Z. Zhao, M. P. J. Lavery,N. Ashrafi, S. Ashrafi, R. Bock, M. Tur, A. F. Molisch, A. E. Willner, Optica **2**, 357-365, 2015.
11. G. Vallone, V. D'Ambrosio, A. Sponselli, S. Slussarenko, L. Marrucci, F. Sciarrino, and P. Villoresi, Phys. Rev. Lett. **113**, 060503 (2014).
12. M. Krenn, R. Fickler, M. Fink, J. Handsteiner, M. Malik, T. Scheidl, R. Ursin, and A. Zeilinger, New J. Phys. **16**, 113028 (2014).
13. J. A. Anguita, H. P. Rodriguez, and M. A. Vial, "Characterization of OAM states affected by turbulence for high-speed short-range links," Proc. of Frontiers in Optics (FiO), paper F5h3b.5, Tucson, Arizona, 2014.
14. M. P. Lavery, B. Heim, C. Peuntinger, E. Karimi, O. S. Magaña-Loaiza, T. Bauer, C. Marquardt, A. Willner, R. W. Boyd, M. Padgett, and G. Leuchs, Proc. of CLEO, paper STu1L.4, San Jose, CA, 2015.
15. Y. Ren, Z. Wang, P. Liao, L. Li, G. Xie, H. Huang, Z. Zhao, Y. Yan, N. Ahmed, M. Lavery, N. Ashrafi, S. Ashrafi, R. Linquist, M. Tur, I. B. Djordjevic, M. Neifeld, and A. Willner, Proc. of OFC, paper M2F.1, Los Angeles, CA, 2015.
16. L. Andrews, and R. Phillips, Laser Beam Propagation through Random Media, 2nd ed., SPIE Press, Bellingham, Washington, 2005.
17. J. A. Anguita, M. A. Neifeld, and B. V. Vasic, Appl. Opt. **47**, 2414-2429 (2008).
18. Y. Ren, H. Huang, G. Xie, N. Ahmed, Y. Yan, B. I. Erkmen, N. Chandrasekaran, M. P. J. Lavery, N. K. Steinhoff, M. Tur, S. Dolinar, M. Neifeld, M. J. Padgett, R. W. Boyd, J. H. Shapiro, and A. E. Willner, Opt. Lett. **38**, 4062-4065 (2013).
19. N. Chandrasekaran and J. H. Shapiro, IEEE J. lightw. Tech. **32**, 1075-1087 (2014).
20. S. Arnon, Opt. Lett. **28**, 129-131 (2003).
21. J. D. Barry, G.S. Mecherle, Opt. Eng. **24**, 1049-1054 (1985).
22. T. Nieelsen, Proc. SPIE, Free-Space Laser Communication Technologies VII **2381**, 194-205 (1995).
23. http://photonic.ws/Free_Space_Optical_Communication_Tip-Tilt-Mirror_Brochure.pdf, pp. 6-7, 2014.
24. Y. Ren, G. Xie, H. Huang, N. Ahmed, Y. Yan, L. Li, C. Bao, M. P. J. Lavery, M. Tur, M. Neifeld, R. W. Boyd, J. H. Shapiro, and A. E. Willner, Optica **1**, 376-382 (2014).

Full References

1. V.W.S. Chan, “Free-space optical communications,” IEEE J. lightw. Tech., vol. 24, no. 11, pp. 4750-4762, 2006.
2. I. B. Djordjevic and M. Arabaci, “LDPC-coded orbital angular momentum (OAM) modulation for free-space optical communication,” Opt. Express, vol. 18, no. 24, pp. 24722-24728, 2010.
3. E. Ciaramella, Y. Arimoto, G. Contestabile, M. Presi, A. D'Errico, V. Guarino, and M. Matsumoto, “1.28-Tb/s (32×40 Gb/s) free-space optical WDM transmission system,” IEEE Photon. Technol. Lett., vol. 21, no. 16, pp. 1121-1123, 2009.
4. A. Turpin, Y. Loiko, T. K. Kalkandjiev, and J. Mompart, “Free-space optical polarization demultiplexing and multiplexing by means of conical refraction,” Opt. Lett., vol. 37, no. 20, pp. 4197-4199, 2012.
5. G. Gibson, J. Courtial, M. Padgett, M. Vasnetsov, V. Pas'ko, S. Barnett, and S. Franke-Arnold, “Free-space information transfer using light beams carrying orbital angular momentum,” Opt. Express, vol. 12, no. 22, pp. 5448-5456, 2004.
6. J. Wang, J.-Y. Yang, I. M. Fazal, N. Ahmed, Y. Yan, H. Huang, Y. Ren, Y. Yue, S. Dolinar, M. Tur, and A. E. Willner, “Terabit free-space data transmission employing orbital angular momentum multiplexing,” Nature Photonics, vol. 6, pp. 488-496, 2012.
7. T. Su, R. P. Scott, S. S. Djordjevic, N. K. Fontaine, D. J. Geisler, X. Cai, and S. J. B. Yoo, “Demonstration of free space coherent optical communication using integrated silicon photonic orbital angular momentum devices,” Opt. Express, vol. 20, no. 9, pp. 9396-9402, 2012.
8. L. Allen, M. W. Beijersbergen, R. J. C. Spreeuw, and J. P. Woerdman, “Orbital angular momentum of light and the transformation of Laguerre-Gaussian laser modes,” Phys. Rev. A, vol. 45, no. 11, pp. 8185-8190, 1992.
9. A. Yao and M. J. Padgett, “Orbital angular momentum: origins, behavior and applications,” Adv. Opt. Photon., vol. 3, no. 2, pp. 161-204, 2011.
10. G. Xie, L. Li, Y. Ren, H. Huang, Y. Yan, N. Ahmed, Z. Zhao, M. P. J. Lavery,N. Ashrafi, S. Ashrafi, R. Bock, M. Tur, A. F. Molisch, A. E. Willner, “Performance metrics and design considerations for a free-space optical orbital-angular-momentum multiplexed communication link,” Optica, vol. 2, no. 4, pp. 357-365, 2015.
11. G. Vallone, V. D’Ambrosio, A. Sponselli, S. Slussarenko, L. Marrucci, F. Sciarrino, and P. Villoresi, “Free-Space Quantum Key Distribution by Rotation-Invariant Twisted Photons,” Phys. Rev. Lett., vol. 113, 060503, 2014.
12. M. Krenn, R. Fickler, M. Fink, J. Handsteiner, M. Malik, T. Scheidl, R. Ursin, and A. Zeilinger, “Communication with spatially modulated light through turbulent air across Vienna,” New J. Phys., vol. 16, 113028, 2014.
13. J. A. Anguita, H. P. Rodriguez, and M. A. Vial, “Characterization of OAM states affected by turbulence for high-speed short-range links,” Proc. of Frontiers in Optics (FiO), paper F5h3b.5, Tucson, Arizona, 2014.
14. M. P. Lavery, B. Heim, C. Peuntinger, E. Karimi, O. S. Magaña-Loaiza, T. Bauer, C. Marquardt, A. Willner, R. W. Boyd, M. Padgett, and G. Leuchs, "Study of Turbulence Induced Orbital Angular Momentum Channel Crosstalk in a 1.6 km Free-Space Optical Link," Proc. of CLEO, paper STu1L.4, San Jose, CA, 2015.
15. Y. Ren, Z. Wang, P. Liao, L. Li, G. Xie, H. Huang, Z. Zhao, Y. Yan, N. Ahmed, M. Lavery, N. Ashrafi, S. Ashrafi, R. Linquist, M. Tur, I. B. Djordjevic, M. Neifeld, and A. Willner, "400-Gbit/s Free Space Optical Communications Link Over 120-meter Using Multiplexing of 4 Collocated Orbital-Angular-Momentum Beams," Proc. of Optical Fiber Communication Conference, paper M2F.1, Los Angeles, CA, 2015.
16. L. Andrews, and R. Phillips, Laser Beam Propagation through Random Media, 2nd ed., SPIE Press, Bellingham, Washington, 2005.
17. J. A. Anguita, M. A. Neifeld, and B. V. Vasic, “Turbulence-induced channel crosstalk in an orbital angular momentum-multiplexed free-space optical link,” Appl. Opt., vol. 47, no. 13, pp. 2414-2429, 2008.
18. Y. Ren, H. Huang, G. Xie, N. Ahmed, Y. Yan, B. I. Erkmen, N. Chandrasekaran, M. P. J. Lavery, N. K. Steinhoff, M. Tur, S. Dolinar, M. Neifeld, M. J. Padgett, R. W. Boyd, J. H. Shapiro, and A. E. Willner, “Atmospheric turbulence effects on the performance of a free space optical link employing orbital angular momentum multiplexing,” Opt. Lett., vol. 38, no. 20, pp. 4062-4065, 2013.
19. N. Chandrasekaran and J. H. Shapiro, “Photon Information Efficient Communication Through Atmospheric Turbulence–Part I: Channel Model and Propagation Statistics,” IEEE J. lightw. Tech., vol. 32, no. 6, pp. 1075-1087, 2014.
20. S. Arnon, "Effects of atmospheric turbulence and building sway on optical wireless-communication systems," Opt. Lett., vol. 28, no. 2, pp. 129-131, 2003.
21. J. D. Barry, G.S. Mecherle, "Beam pointing error as a significant design parameter for satellite-borne, free-space optical communication systems," Opt. Eng., vol. 24, no. 6, pp. 1049-1054, 1985.
22. T. Nieelsen, "Pointing, acquisition, and tracking system for the free-space laser communication system SILEX," Proc. SPIE, Free-Space Laser Communication Technologies VII, vol. 2381, pp. 194-205, 1995.
23. http://photonic.ws/Free_Space_Optical_Communication_Tip-Tilt-Mirror_Brochure.pdf, pp. 6-7, 2014.
24. Y. Ren, G. Xie, H. Huang, N. Ahmed, Y. Yan, L. Li, C. Bao, M. P. J. Lavery, M. Tur, M. Neifeld, R. W. Boyd, J. H. Shapiro, and A. E. Willner, "Adaptive-optics-based simultaneous pre- and post-turbulence compensation of multiple orbital-angular-momentum beams in a bidirectional free-space optical link," Optica, vol. 1, no. 6, pp. 376-382, 2014.